Advances in Science and Technology Research Journal

Advances in Science and Technology Research Journal, 2026, 20(4), 260–270
https://doi.org/10.12913/22998624/214948
ISSN 2299-8624, License CC-BY 4.0

Received: 2025.10.29
Accepted: 2025.02.15
Published: 2026.03.01

Radiometric data compensation methods for dynamic temperature recording

Karol Grochalski[1*], Marcin Białek[2]

[1] Institute of Mechanical Technology, Division of Metrology and Measurement Systems, Poznan University of Technology, Faculty of Mechanical Engineering, ul. Piotrowo 3, Poznan 60-965, Poland
[2] Faculty of Mechanical Engineering, Institute of Mechanical Technology, Division of Mechatronic Devices, Poznan University of Technology, ul. Piotrowo 3, Poznan 60-965, Poland
* Corresponding author's e-mail: karol.grochalski@put.poznan.pl

ABSTRACT

Infrared thermography inspection has become increasingly valuable for assessing various materials and structures in non-destructive testing and evaluation applications. This study investigates the challenges and methodologies associated with thermographic measurement of moving objects, with a particular focus on the impact of motion speed and object size on temperature reading accuracy. To address the issue of image distortion caused by motion, a pixel-shifting compensation algorithm was developed, which corrects the distortion of the thermal image caused by the motion of the object. The proposed method enables the identification and extraction of areas with elevated temperatures (artifacts), even under conditions of dynamic scene changes. The results demonstrate the potential for isolating moving objects from thermal backgrounds, even at high speeds. Despite the decrease in the number of visible frames as velocity increases, the method proved effective in reliably identifying and tracking thermal signatures. Further investigation will be conducted to refine the relationship between shift factor and object velocity, particularly in the non-linear regime, to enhance the robustness of compensation methods for high-speed thermographic inspections.

Keywords: thermography, radiometric compensation, pixel-shifting algorithm, dynamic thermal imaging, non-destructive testing.

INTRODUCTION

Infrared thermography inspection has become increasingly valuable for assessing various materials and structures in non-destructive testing and evaluation (NDT&E) applications [1]. It has been applied to infrastructure [2], composite-metal structures [3], aircraft structures [4], and carbon fiber reinforced polymer (CFRP) materials [5,6]. To accommodate the inspection of large-scale components, researchers have introduced techniques such as laser spot thermography (LST) with narrow line excitation and flying line configurations [7]. These configurations involve the movement of the excitation source across the field of view (FOV– the viewing angle of the entire optical system of the camera, i.e. how wide the camera sees the scene) at a constant speed [8]. In some studies, a two-step approach has been proposed for data reconstruction in LST: first, extracting temperature series features such as maximum temperature for each pixel, and second, aligning the starting points of each time series according to the maximum temperature [9]. However, limitations persist, particularly regarding the fixed and limited FOV. To address this limitation, scientists have explored moving both the camera and the excitation source [10]. This approach presents challenges in data reconstruction due to the motion of the FOV. The pseudo-static motion reconstruction (PSMR) method has been proposed to process data captured in [11], performed by translating each frame by an integer number of pixels. PSMR-based algorithms assume a constant integer motion speed,

which may not hold true in practice. Attempts to address this issue include estimating velocity using laser beam or object edge features. To optimize reconstruction algorithms and enhance defect detection in LST, the line-scanning thermography reconstruction (LSTR) algorithm has been proposed [8]. LSTR utilizes velocity mapping and spatial interpolation techniques to align scanning data spatially and temporally, resulting in improved defect detection rates. Additional methods such as CNN-based thermographic analysis [12,13], super-resolution laser line scanning [14], and compensation of measurement interferences [15] have further extended the capabilities of LST techniques. Furthermore, hybrid approaches combining thermography with optical metrology [16] or implementing filtered contrast techniques [17] have demonstrated enhanced accuracy in defect characterization. In summary, infrared thermography offers significant potential for NDT&E applications across various materials and structures. Advancements in techniques such as LST, PSMR-based algorithms, and hybrid methodologies have led to improved defect detection capabilities, but challenges remain in achieving accurate and efficient data reconstruction. Further research is needed to address these challenges and unlock the full potential of infrared thermography in NDT&E.

Thermographic examination of moving objects presents unique challenges due to the dynamic nature of the inspection process. Traditional thermography methods are often optimized for stationary objects, where the camera and the object remain relatively still during data acquisition. However, when dealing with moving objects, such as machinery components or vehicles, several factors need to be considered to ensure accurate and reliable thermographic inspections. Based on the literature review, several areas of concern were identified:

One of the primary challenges in thermographic examination of moving objects is motion blur. The movement of the object during image acquisition can result in blurred thermal images, reducing the clarity and quality of the captured data. To mitigate motion blur, specialized techniques such as high-speed thermography or synchronization of camera exposure with object motion may be employed. These techniques help to minimize the effects of motion blur and improve the overall quality of thermal images.

Another consideration is the synchronization of thermal data acquisition with the motion of the object. In applications where precise temperature measurements are required, it is essential to ensure that thermal images are captured at the right moment in the object's motion cycle. This may involve triggering the camera based on motion sensors or integrating thermal imaging systems with the object's control system for real-time synchronization.

Furthermore, the analysis of thermal data from moving objects may require advanced signal processing techniques to account for variations in object motion and temperature distribution. Algorithms for motion compensation, image registration, and temporal analysis may be employed to accurately analyze thermal data captured from moving objects and detect anomalies or defects.

MATERIALS AND METHODS

Accurate non-contact temperature measurement requires determining the emissive properties of the examined surface, defining the observation angle, and assessing whether the object is stationary or in motion. The emissivity coefficient (ε), one of the most crucial factors in non-contact measurements, depends on the material composition of the object as well as the texture of its surface. Additionally, these factors are influenced by the temperature of the measured object.

To minimize the impact of external factors when analyzing the effect of motion speed on dynamic temperature measurements, the study employed an autonomous blackbody emitter PCO TW88/Zs2 (Figure 1b) with a known surface emissivity of $\varepsilon = 0.98$. This device allowed for precise temperature control across the entire measurement surface. The system enabled accurate temperature settings in the range of 27 °C to 50 °C, with a precision of better than 0.1 °C. Furthermore, the emitter was equipped with a slit aperture mount, which facilitated the evaluation of the camera's detection capabilities for small objects or those with limited radiative capacity, whether stationary or in motion.

In thermographic techniques, a blackbody serves as a reference standard for accurate temperature measurement. By conducting both static and dynamic measurements with a reference source, it is possible to minimize disturbances that could affect the accurate determination of parameters compensating for dynamic factors in the conducted measurements. For the purpose of this study, a FLIR T620 thermal imaging camera

was used, featuring a 640 × 480 pixel sensor. In terms of spatial (geometric) resolution, its instantaneous field of view (IFOV – the viewing angle of a single detector pixel of the thermal camera / optical system) is 0.62 milliradians, while its thermal resolution, defined as the noise equivalent temperature difference (NETD). It is the smallest temperature difference between the object and the background that the thermal camera is able to register with a signal equal to the detector's own noise level), is 0.05 °C. It should also be noted that NETD depends on several factors, such as ambient temperature, detector wavelength, and the noise level of the camera's electronics. The maximum measurement error of the device is ±2 °C or ±2% of the recorded temperature, with the greater of these two values being considered the limiting error.

To ensure the accuracy of the camera's readings and its proper calibration, independent temperature reference sources LAND P550P and LAND P80P were used, both holding valid calibration certificates. Measurement accuracy was assessed after the thermal stabilization of both the camera and the reference sources, maintained in a static state. This approach aimed to minimize measurement errors and correctly determine both actual and apparent temperatures on the moving thermal emitter.

The temperature of the radiator was measured in such a way that the thermal imaging camera observed the object with its deviation angle from the optical axis not exceeding 30°, and the radiator was positioned as close as possible to ensure the required geometric resolution. The data recording frequency for a full frame is defined as 30 Hz (the maximum recording frequency for the implemented bolometric detector of the applied thermal imaging camera). Thermograms were analyzed using FLIR ResearchIR MAX software, which allows for determining the influence of velocity on accurate temperature readings and defining a compensation curve (provided that the surface temperature is known).

The temperature radiator was mounted on the UR3 robot, and its trajectory followed a straight line. The movement distance of the radiator was 1 meter (excluding the section required for the robot arm to decelerate and accelerate), as schematically shown in the figure (Figure 1a). The robot performed six passes in each direction for every test (12 readings on the thermogram). The linear movement speed (preset) was defined in the range of 200–1400 mm/s. The set temperature on the surface of the radiator was 50 °C. The test stand is shown in Figure 1c.

Figure 2 shows the blackbody radiator in the two test scenarios considered. The situation analysed is one in which there is full exposure of the radiator (Figure 2a) and one in which an aperture is applied to the radiator to limit the emission of thermal radiation (Figure 2b). Provided aperture was a screen with a two 2 mm slots. This approach allows for measurements when the tested object is small in size or located at a significant distance from the thermal camera (assuming negligible atmospheric attenuation).

The raw data was acquired using the software Flir Tools. It allows the generation of a file with a.csv extension containing the individual frames of the camera footage. The data structure consists of a column containing the frame number and the relevant number of columns and rows corresponding to the resolution of the recorded image. In

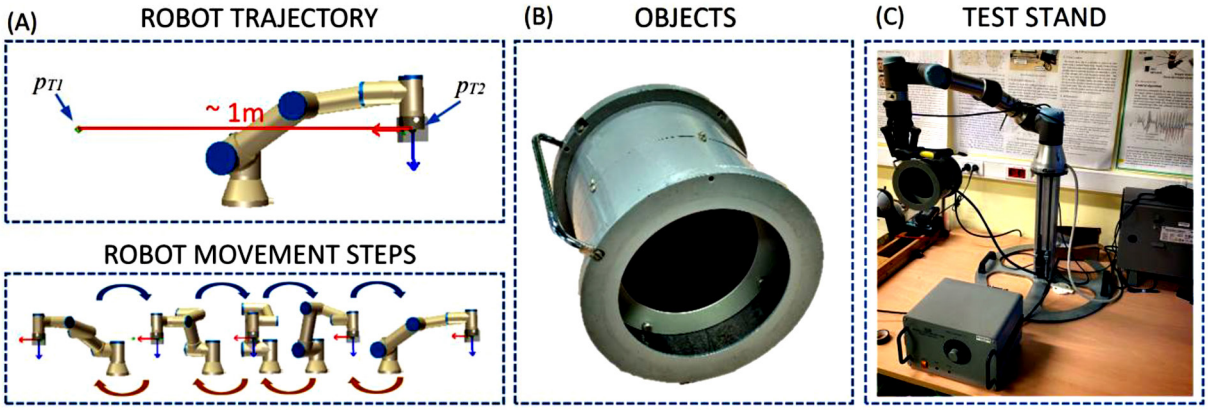

Figure 1. Measurement setup for studying the impact of movement speed on non-contact temperature reading: (a) robot arm with designated motion trajectory, (b) blackbody radiator PCO TW88/Zs2, c) robot arm with mounted blackbody emitter

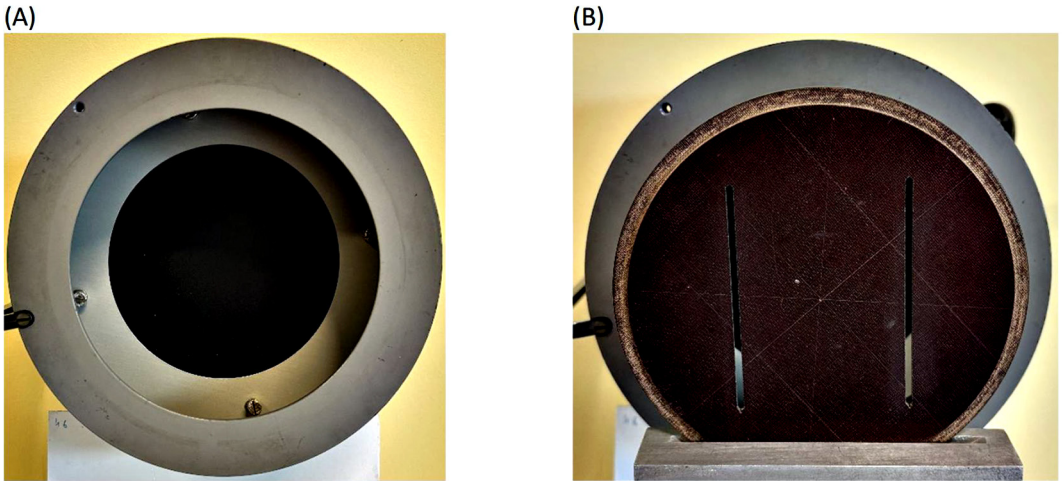

Figure 2. Two blackbody test scenarios: (a) radiator without aperture, (b) radiator with aperture

this case 300 × 300 px (pixels). The data in the individual cell contains an indication of the temperature (Figure 3). A Python script was written to extract the data from the file and save it as a Pandas dataframe, for further analysis. Figure 3 shows an example of two frames containing a heatmap visualisation of the data. One may observe that the recorded image of an object in motion is distorted. For this reason, this article proposes some methods for analysing the acquired data and the possibilities for image data compensation.

RESULTS

Static temperature measurements

In the first part of the study, the temperature was measured in a static state for the radiator without a slot screen (Figure 4a), and then a screen with a 2 mm slot was installed (Figure 4b). The measurement area emits infrared radiation across its entire surface, and the radiation is not attenuated. Illustration (Figure 4b) presents a thermal image of the CDC radiator, where the radiation passing through the screen is attenuated, and the recorded temperature values are lower than the reference value. The difference in readings is $\Delta T_{ref}(o\text{-}s) = 4.7\ °C \pm 0.1\ °C$.

The radiator without a screen was used as a measurement variant when the tested object (either stationary or in motion) was sufficiently large to minimize the influence of the thermal camera's geometric resolution on the temperature reading. The addition of a slot screen is a study variant that allows for the determination of its effect in situations where the tested object is very small or located far from the thermal camera, and the infrared radiation emission is attenuated.

Dynamic temperature measurements

The plots in Figure 5 present the recorded temperature values of the blackbody radiator in motion for selected linear velocities in the range of 200–1400 mm/s.

When analyzing the temperature readings as a function of the linear velocity of the radiator's motion, it should be noted that for large objects, which can be observed over a significant area of the infrared detector, the

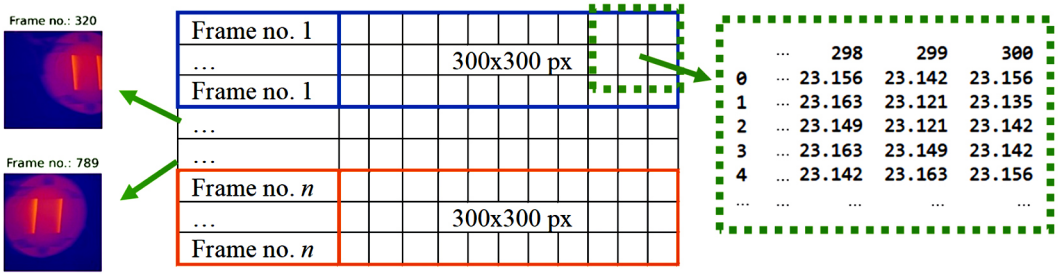

Figure 3. Raw data structure – the individual frames of the captured camera footage

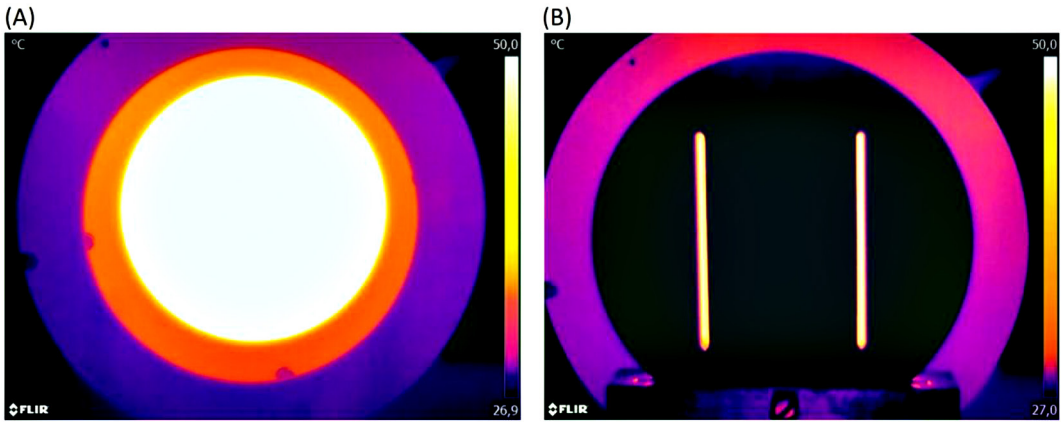

Figure 4. Reference temperature values for a blackbody radiator in static condition: a) radiator without aperture $T_{ref}(o)$ = 50 °C ± 0.1 °C, b) radiator with aperture $T_{ref}(s)$ = 45.3 °C ± 0.1 °C

temperature drop is minimal—approximately 0.3 °C (within the tested velocity range) with a monotonic linear trend (Figure 5a). Furthermore, the graph indicates the standard deviation of the measured values, equal to 0.12 °C (Figure 5c). This value meets the noise equivalent temperature difference criterion while remaining within the acceptable error margin of the thermal camera. The standard deviation value in this study variant is fundamental to understanding the nature of temperature readings in motion (dynamic state). If the standard deviation remains constant regardless of the object's velocity and has a low value, this state can be interpreted as stable and undisturbed, indicating that the thermogram contains sufficient radiometric information for accurate surface temperature determination. Another key observation is that the measured temperature of the moving CDC surface (above the threshold velocity for a given thermal camera) is lower than the reference temperature recorded in the static

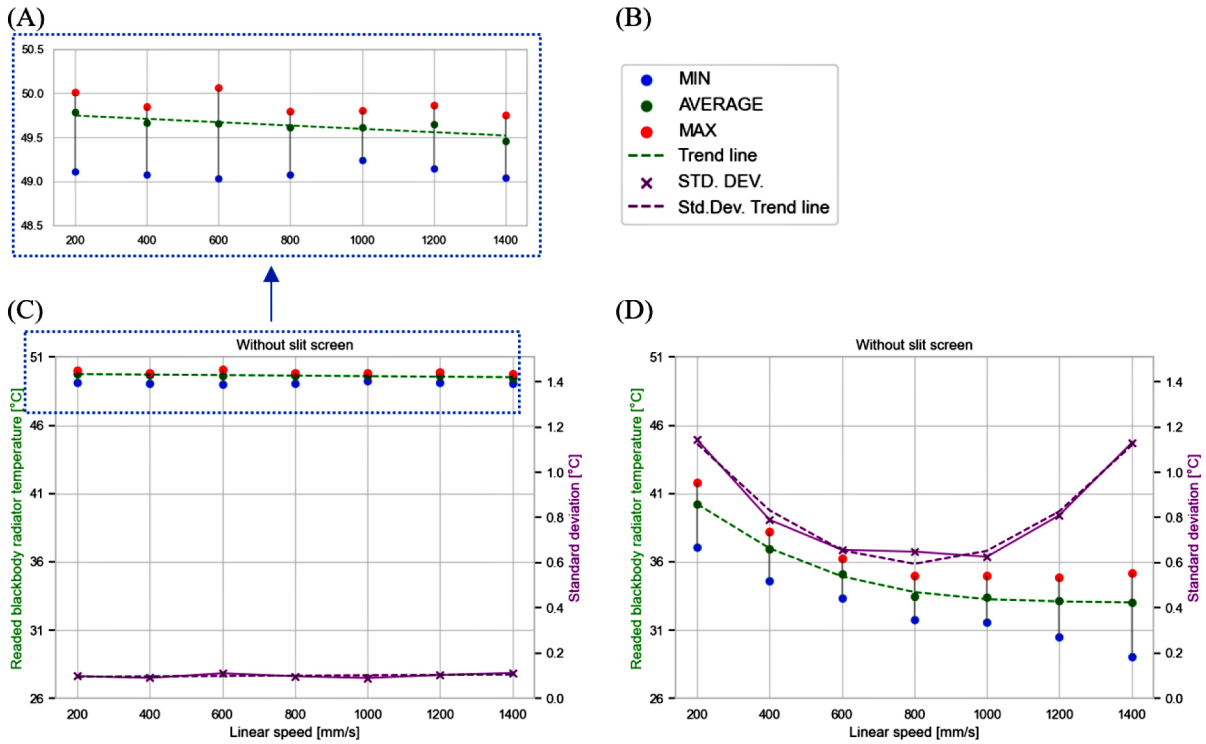

Figure 5. Plots of temperature values for an emitter in a dynamic state: (a) without slit screen – a close-up view on the range of interest, (b) legend, (c) without slit screen T_{ref} = 50 °C ± 0.1 °C, (d) with slit screen T_{ref} = 45.3 °C ± 0.1 °C

state (Figure 4). This effect may be associated with the averaging of radiance on the bolometric matrix or thermal image blurring. Based on the graph, it can also be concluded that for objects captured over a large area of the thermal camera's detector matrix, motion velocity has a minimal impact on disturbances and the accuracy of temperature readings, as confirmed by the standard deviation analysis.

Figure 5d shows the second variant of the study, in which a slot screen was placed on the infrared radiator. The screen significantly reduces the amount of radiation reaching the thermal camera. As mentioned in the methodology (section 2), this approach allows for measurements when the tested object is small in size or located at a significant distance from the thermal camera (assuming negligible atmospheric attenuation). It should be noted that as the velocity increases, the temperature value recorded from the thermogram decreases. This relationship follows a exponential pattern in the considered boundary values of the experiment. The range of temperature differences between the static state of the CDC radiator with the screen and the dynamic state falls within the range of 5.1 °C to 12.4 °C.

An important insight comes from the analysis of the standard deviation. The trend follows a power-law characteristic, which clearly indicates greater variability in the recorded data, and thus, increased disturbances. A noticeable increase in the standard deviation—disturbances occurs above a motion speed of 1000 mm/s. This effect is closely related to the amount of data recorded by the bolometric detector, as well as the bolometer's response frequency limit to changes in infrared radiation. The amount of data—radiation is limited by the physical screen, which also affects the thermal camera's geometric resolution capabilities. Based on the graph, it can be concluded that for small objects, the motion velocity plays a significant role in the accuracy of the temperature reading. Additionally, the measured temperature is significantly lower than the reference value.

Data compensation methods

Figure 6 presents the results of applying the developed artifact extraction algorithm to raw thermographic data recorded for a moving object with a velocity of 200 mm/s. The proposed method enables the identification and extraction of areas with elevated temperatures (artifacts) from individual frames of the thermal sequence.

Figure 6a shows a reference frame (frame no. 100) acquired in the absence of the moving object. The thermogram remains uniform without any temperature gradients indicating the object's presence. Figure 6b presents five consecutive frames (frames no. from 313 to 317) in which the object passes through the camera's field of view. The extracted artifacts, corresponding to the areas of increased temperature, are clearly visible and follow the shape and position of the moving object. Figure 6c illustrates the trend of the average temperature calculated for each frame across the entire recorded sequence. Distinct periodic peaks are observed, which correspond to the successive appearances of the moving object in the scene. The dashed orange line represents a predefined temperature threshold applied in the artifact detection process. Each peak exceeding this threshold indicates the presence of the object with higher surface temperature compared to the background. Figure 6d provides the applied temperature scale range, used for thermogram visualization. Selected frames with the highest recorded average temperature values are shown in Figure 6e. These frames correspond to the moments when the moving object is fully visible within the scene. The effectiveness of the algorithm in isolating the object from the background is confirmed by the consistent shape, size, and position of the detected artifacts across the entire sequence.

Figure 7 presents the results of the artifact extraction algorithm applied to thermographic data of a moving object at a velocity of 1400 mm/s. The increased speed of the object significantly affects the characteristics of the recorded thermal signal. The observed peaks are sharper and narrower, corresponding to the brief presence of the object in the camera's field of view (Figure 7c). The applied threshold (orange dashed line) enables effective detection of frames containing the object despite its rapid movement. Despite the high velocity, the artifact extraction algorithm effectively identifies the object's location and shape in each frame (Figure 7e).

The results confirm the robustness of the proposed method in processing thermographic data of fast-moving objects. The algorithm allows for reliable detection and isolation of thermal artifacts even under conditions of dynamic scene changes. For the object moving at a velocity of 1400 mm/s (Figure 7), the detected thermal

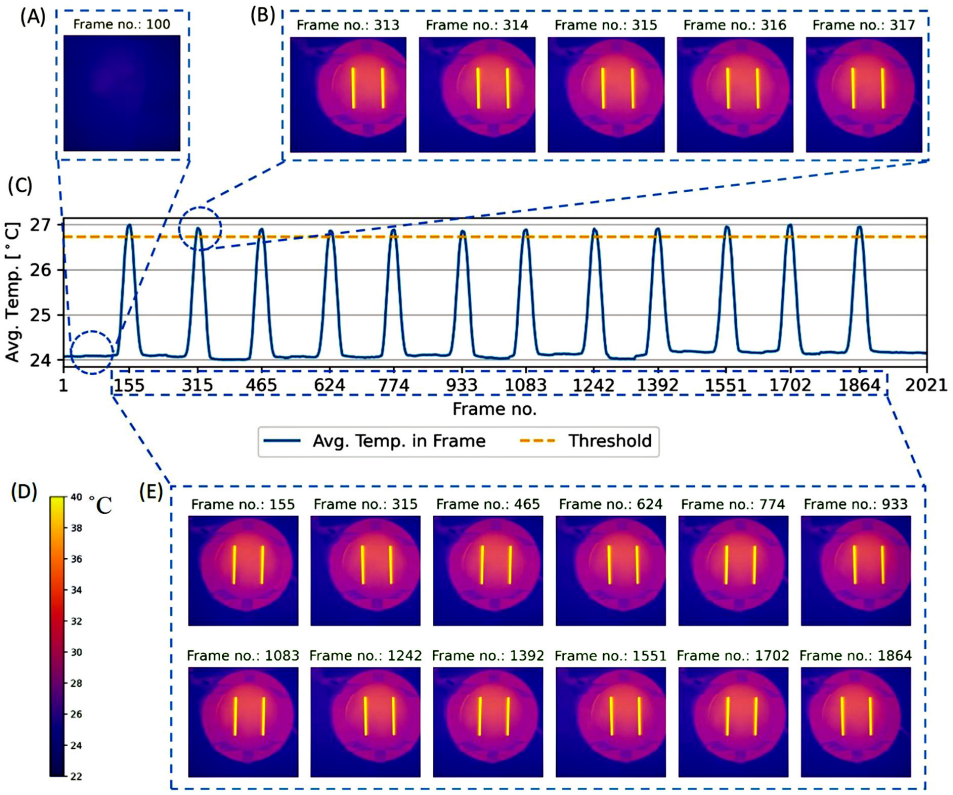

Figure 6. Motion velocity 200 mm/s: (a) frame without object, (b) 5 consecutive frames with object, (c) graph of average temperature value in frames, (d) colour scale of thermogram, (e) frames with highest average temperature (with detected objects)

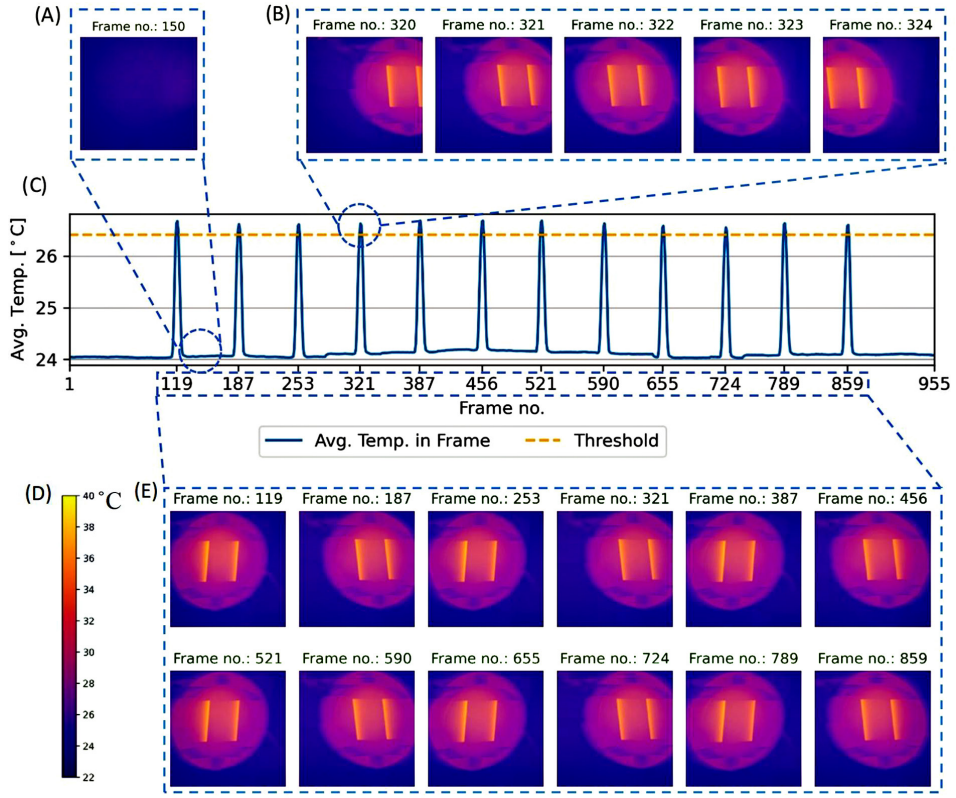

Figure 7. Motion velocity 1400 mm/s: (a) frame without object, (b) 5 consecutive frames with object, (c) graph of average temperature value in frames, (d) colour scale of thermogram, (e) frames with highest average temperature (with detected objects)

artefacts are noticeably narrower and deformed compared to the lower velocity case (Figure 6). This results from the significantly shorter exposure time of the object within a single frame. In the following part of the article, a method for image distortion compensation will be presented to reconstruct the actual shape and dimensions of the moving object.

Figure 8 presents the relationship between the object velocity and the average number of recorded frames containing the moving object (artifact). As expected, the higher the velocity of the moving object, the smaller the number of frames in which the object is visible. This effect is directly related to the motion dynamics and the temporal resolution of the recording system.

The results clearly indicate that for low object velocities (below approximately 400 mm/s), the number of frames capturing the object is relatively high. However, for higher velocities, the average frame count decreases rapidly, and for velocities exceeding 1000 mm/s it stabilizes at a minimum level. This observation is crucial from the perspective of radiometric compensation methods, as it highlights the limitations of using static correction models in dynamic scenarios.

The proposed image compensation algorithm is based on a pixel-shifting method, which corrects the distortion of the thermal image caused by the motion of the object. As shown in Figure 9, the original frame (left) contains a deformed thermal image of the moving object due to its relative displacement during the exposure time. The compensation process involves shifting the pixels in the frame along the direction of motion to restore the correct geometry of the object.

The shifting amount for each row of pixels is determined by the so-called "Frame Shifting Curve" (middle), which describes the relationship between the pixel shift amount and the vertical position in the frame. The slope of this curve depends on the velocity of the moving object and the camera parameters (e.g., frame rate, exposure time).

$$s_w = s_f \cdot h_O \tag{1}$$

where: s_w is the shift amount applied to each row [px], s_f is the maximum shift factor applied to the top row [-], h_0 is the row index, starting from 0 for the top row [px].

As a result of the applied shifting operation (right), the image is corrected, and the object regains its original, undistorted shape. The bottom part of the figure illustrates a schematic representation of the shifting process, where the pixels in each row are moved by a specific amount according to the calculated shift vector. This method enables accurate reconstruction of the object's geometry in the thermal image despite its motion during the recording.

The results presented in Figure 10 demonstrate a clear dependency between the shift factor and the object velocity. In order to describe the observed behavior, two approximation functions of shift

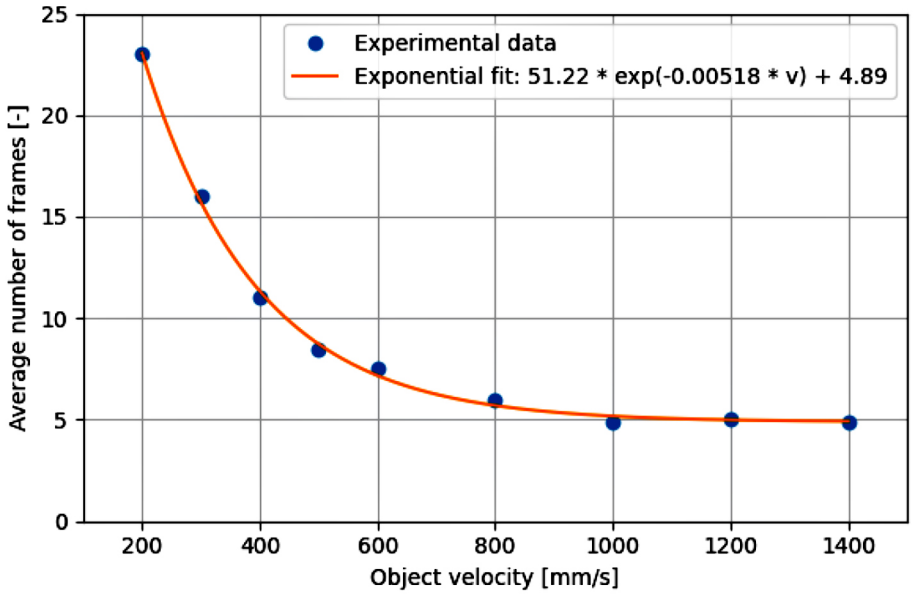

Figure 8. The average number of consecutive frames containing the moving object recorded in relation to its velocity

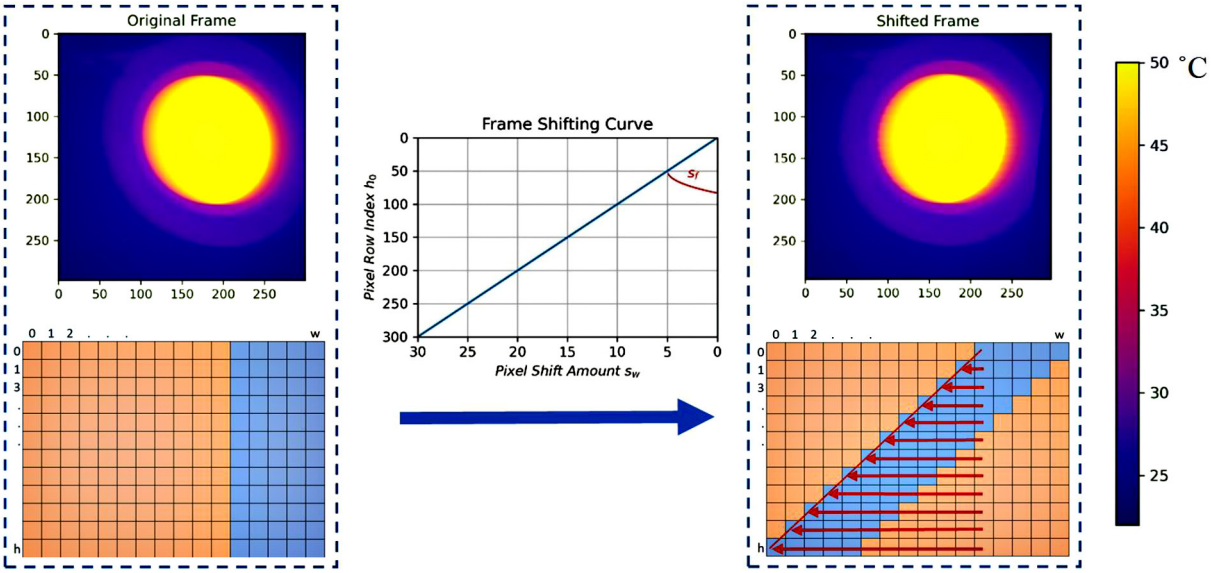

Figure 9. Schematic representation of the image distortion compensation algorithm based on the pixel-shifting method: (left) original distorted frame, (middle) frame shifting curve defining the shift amount for each row depending on the object velocity, (right) corrected (shifted) frame with restored object geometry

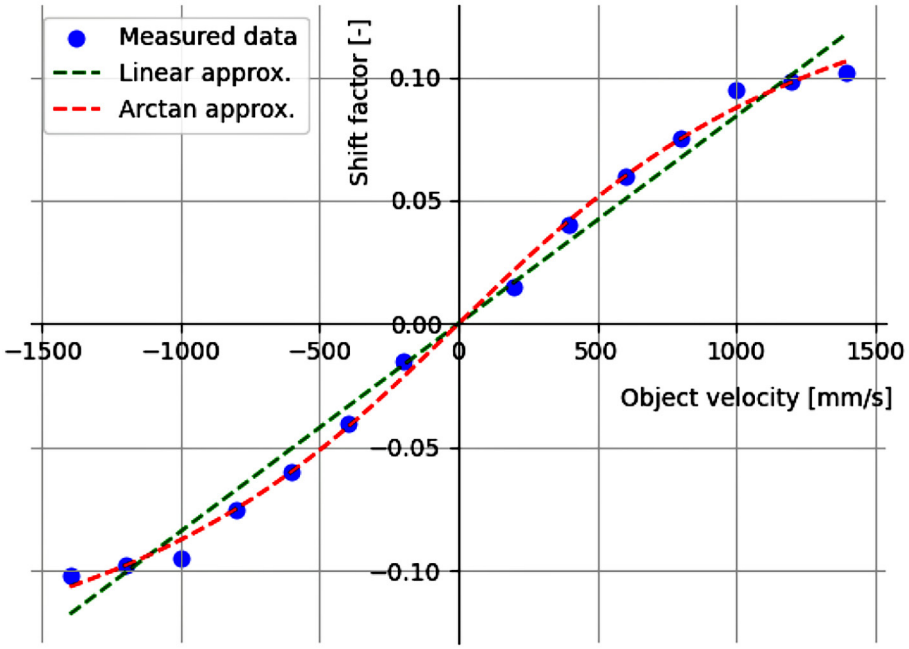

Figure 10. Relationship between the shift factor used in the compensation algorithm and the object velocity. The initial section exhibits a linear trend, whereas for higher velocities the function tends to flatten. This behaviour suggests the applicability of non-linear functions (e.g., tangent or logarithmic) for shift factor approximation

factor $SF(V)$ [-] were proposed. For lower velocities, the relationship remains approximately linear, which suggests the possibility of using a simplified linear compensation model in this range:

$$SF(V) = a \cdot V + b \tag{2}$$

However, as the object velocity increases, the relation tends to saturate, and the shift factor grows non-linearly, based on the tangent:

$$SF(V) = A \cdot \tan(B \cdot V) \tag{3}$$

where: a, b, A, B – constants fitted to the experimental data [-].

The usage of the tangent function allows capturing the rapid increase of the shift factor for intermediate velocities, while simultaneously reflecting the saturation effect for higher velocities. This type of function appears to be particularly

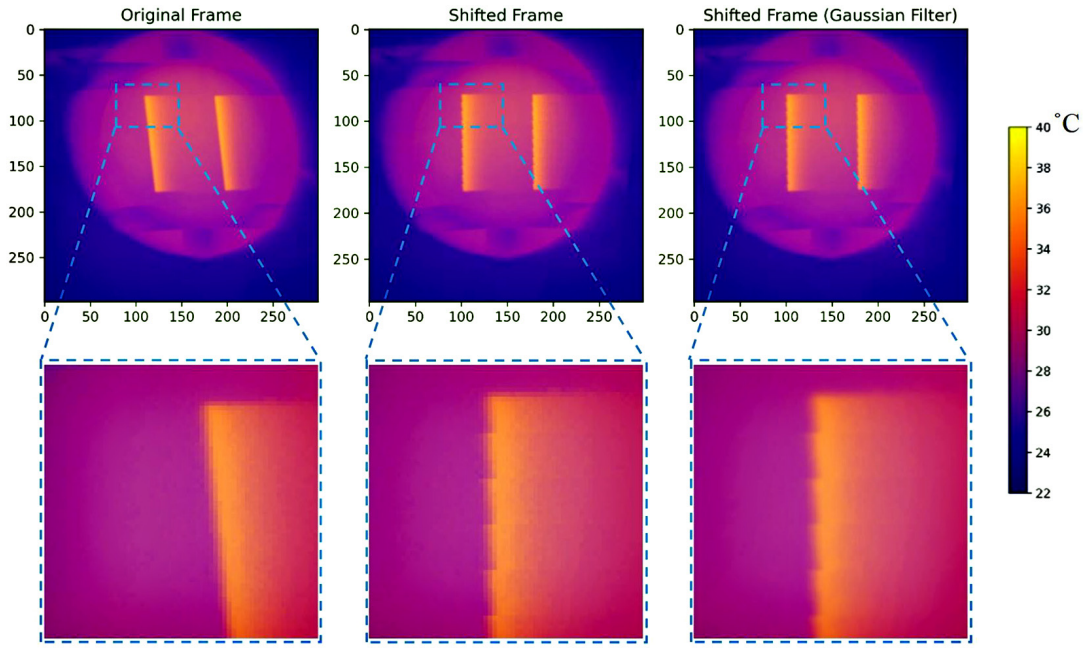

Figure 11. Shifted frame interpolation

suitable for dynamic scenarios with varying motion speeds. Figure 11 presents an example of the object image processing steps used in the proposed method. The left image shows the original thermographic frame captured during the experiment. The middle image presents the result of the frame shifting operation used for motion compensation. The right image shows the final result after applying a Gaussian filter to smooth the discontinuities caused by the shifting process. The zoomed-in regions highlight the improvements in edge continuity and temperature distribution achieved after the filtering operation.

CONCLUSIONS

This study investigated the challenges and methodologies associated with thermographic measurement of moving objects, with a particular focus on the impact of motion speed and object size on temperature reading accuracy. A fully automated measurement process was developed, enabling precise, repeatable, and consistent data acquisition using a calibrated blackbody source and a high-resolution thermal imaging camera.

The results clearly indicate that large objects, occupying a significant area of the detector matrix, can be thermographically analyzed while in motion with minimal loss of temperature reading accuracy. In such cases, the temperature drop remains small and follows a nearly linear trend with increasing speed, with the standard deviation of temperature readings staying within the acceptable limits of the system's NETD. Conversely, when observing small objects—especially through a limited aperture—the accuracy of thermographic measurements degrades significantly with increasing speed. In these conditions, the recorded temperature decreases noticeably, and the data variability increases, particularly above 1000 mm/s. This highlights the importance of geometric resolution and exposure time in capturing accurate thermal information from fast-moving, small-sized objects.

To address the issue of image distortion caused by motion, a pixel-shifting compensation algorithm was developed. This method corrects the geometric deformation of thermal images by shifting pixel rows according to a shift factor derived from the object's velocity. The relationship between the shift factor and the velocity was modeled using both linear and non-linear functions. While a linear approximation suffices for lower speeds, a tangent-based model more accurately describes the behavior at higher velocities, capturing the saturation trend observed in the experimental data. The artifact extraction algorithm developed in this study further demonstrates the potential for isolating moving objects from thermal backgrounds, even at high speeds. Despite the decrease in the number of visible frames as velocity

increases, the method proved effective in reliably identifying and tracking thermal signatures.

Future work will focus on defining the critical speed limit beyond which temperature measurements become unreliable, and determining the minimum object size that can be accurately captured under both static and dynamic conditions. Additionally, further investigation will be conducted to refine the relationship between shift factor and object velocity, particularly in the non-linear regime, to enhance the robustness of compensation methods for high-speed thermographic inspections.

REFERENCES

1. Bagavathiappan, S., Lahiri, B. B., Saravanan, T., Philip, J., Jayakumar, T. Infrared thermography for condition monitoring – A review. Infrared Physics & Technology, 2013; 60, 35–55. https://doi.org/10.1016/j.infrared.2013.03.006
2. Tomita, K., Chew, M. Y. L. A review of infrared thermography for delamination detection on infrastructures and buildings. Sensors, 2022; 22(2), 423. https://doi.org/10.3390/s22020423
3. Chulkov, A. O., Vavilov, V. P., Shagdyrov, B. I., Kladov, D. Y. Automated detection and characterization of defects in composite-metal structures by using active infrared thermography. Journal of Nondestructive Evaluation, 2023; 42, 20. https://doi.org/10.1007/s10921-023-00929-x
4. Farmaki, S., Exarchos, D. A., Tragazikis, I. K., Matikas, T. E., Dassios, K. G. A Novel infrared thermography sensing approach for rapid, quantitative assessment of damage in aircraft composites. Sensors, 2020; 20(15), 4113. https://doi.org/10.3390/s20154113
5. Li, Y., Zhang, W., Yang, Z. W., Zhang, J. Y., Tao, S. J. Low-velocity impact damage characterization of carbon fiber reinforced polymer (CFRP) using infrared thermography. Infrared Physics & Technology, 2016; 76, 91–102.
6. Montesano, J., Fawaz, Z., Bougherara, H. Use of infrared thermography to investigate the fatigue behavior of a carbon fiber reinforced polymer composite. Composite Structures, 2013; 97, 76–83. https://doi.org/10.1016/j.compstruct.2012.09.046
7. Li, T., Almond, D. P., Rees, D. A. S. Crack imaging by scanning laser-line thermography and laser-spot thermography. Measurement Science and Technology, 2011; 22(3), 035701. https://doi.org/10.1088/0957-0233/22/3/035701
8. Deng, B., Li, X., Wang, H., He, Y., Ciampa, F., Li, Y., Zhou, K. Line scanning thermography reconstruction algorithm for defects inspection with novel velocity estimation and image registration. IEEE sensors journal, 2020; 21(10), 11555–11568. https://doi.org/10.1109/JSEN.2020.3034460
9. Santoro, L., Sesana, R. A pilot study using flying spot laser thermography and signal reconstruction. Optics and Lasers in Engineering, 2025; 188, 108901. https://doi.org/10.1016/j.optlaseng.2025.108901
10. Liu, H., Tinsley, L., Deng, K., Wang, Y., Starr, A., Chen, Z., Zhao, Y. A fiber-guided motorized rotation laser scanning thermography technique for impact damage crack inspection in composites. IEEE Transactions on Industrial Electronics, 2023; 71(3), 3163–3172. https://doi.org/10.1109/TIE.2023.3265034
11. Moran, J., Rajic, N. Remote line scan thermography for the rapid inspection of composite impact damage. Composite structures, 2019; 208, 442–453. https://doi.org/10.1016/j.compstruct.2018.10.038
12. Trejo-Chavez, O., Cruz-Albarran, I. A., Resendiz-Ochoa, E., Salinas-Aguilar, A., Morales-Hernandez, L. A., Basurto-Hurtado, J. A., Perez-Ramirez, C. A. A CNN-based methodology for identifying mechanical faults in induction motors using thermography. Machines, 2023; 11(7), 752. https://doi.org/10.3390/machines11070752
13. Bu, C., Shen, R., Bai, W., Chen, P., Li, R., Zhou, R.,..., Tang, Q. CNN-based defect detection and classification of PV cells by infrared thermography method. Nondestructive Testing and Evaluation, 2025; 40(5), 1752–1769. https://doi.org/10.1080/10589759.2024.2357240
14. Ahmadi, S., Burgholzer, P., Jung, P., Caire, G., Ziegler, M. Super resolution laser line scanning thermography. Optics and Lasers in Engineering, 2020; 134, 106279. https://doi.org/10.1016/j.optlaseng.2020.106279
15. Pan, D., Jiang, Z., Li, Y., Yu, H., Gui, W. Intelligent compensation method of infrared temperature measurement for multiple interference factors. IEEE Sensors Journal, 2022; 22(19), 18550–18559. https://doi.org/10.1109/JSEN.2022.3199264
16. Donadello, S. Hybrid optical sensor for combined thermal and dimensional monitoring in laser processing. IEEE Sensors Journal. 2024. https://doi.org/10.1109/JSEN.2024.3477278
17. Gryś, S. Filtered thermal contrast based technique for testing of material by infrared thermography. Opto-Electronics Review, 2011; 19, 234–241. https://doi.org/10.2478/s11772-011-0009-3